Prediction of Trabecular Bone Anisotropy from Quantitative Computed Tomography using Supervised Learning and a Novel Morphometric Feature Descriptor

Vimal Chandran, Philippe Zysset, and Mauricio Reyes

Institute for Surgical Technology and Biomechanics, University of Bern, Swizerland
{vimal.chandran,philippe.zysset,mauricio.reyes}@istb.unibe.ch

Abstract. Patient-specific biomechanical models including local bone mineral density and anisotropy have gained importance for assessing musculoskeletal disorders. However the trabecular bone anisotropy captured by high-resolution imaging is only available at the peripheral skeleton in clinical practice. In this work, we propose a supervised learning approach to predict trabecular bone anisotropy that builds on a novel set of pose invariant feature descriptors. The statistical relationship between trabecular bone anisotropy and feature descriptors were learned from a database of pairs of high resolution QCT and clinical QCT reconstructions. On a set of leave-one-out experiments, we compared the accuracy of the proposed approach to previous ones, and report a mean prediction error of 6% for the tensor norm, 6% for the degree of anisotropy and 19° for the principal tensor direction. These findings show the potential of the proposed approach to predict trabecular bone anisotropy from clinically available QCT images.

Keywords: Trabecular anisotropy, QCT, HRpQCT, Implicit coordinate system, Tensor, Multi-output regression.

1 Introduction

Musculoskeletal diseases, such as osteoporosis, are characterized by low bone mass and impaired trabecular structure, leading to bone fragility and an increased risk for fractures. An improved fracture risk assessment is provided by evaluating the patient's bone strength at an anatomical site at risk (spine, hip) via clinical quantitative computer tomography (QCT)-based finite element analyses [1]. These models can be improved. Indeed, trabecular bone anisotropy, the most important determinant of the mechanical behaviour of trabecular bone after bone volume fraction [2], can be accounted for in numerical simulations to better predict bone strength [3, 4]. Unfortunately, such information is derived from high resolution peripheral QCT (HRpQCT) and is not directly available for the axial skeleton from clinical CT.

Predicting trabecular bone anisotropy using prior knowledge from QCT images has been of interest and two types of strategies have been proposed in

the literature. Firstly, Hazrati-Marangalou et al. [4], proposed a registration driven prediction mechanism. From a database of HRpQCT images, the closest to the patient's image was chosen by minimizing the root-mean-square error and trabecular bone anisotropy was mapped by a mesh morphing technique. Taghizadeh et al. [5], used a template based morphing mechanism where the patient's QCT image was rigidly and non-rigidly registered with a QCT template image. The computed registration transformation was then applied to the corresponding HRpQCT template image to map trabecular bone anisotropy. Although the registration-based approaches have shown good performance, in practice they are computationally expensive and careful registration parameter tuning is required.

A second group of approaches are based on supervised learning. Lekadir et al. [6] used a statistical predictive model, constructed from a database of HRpQCT images. A partial least square (PLS) regression model was built from training data to predict trabecular bone anisotropy. Their approach involves a linear regression and a non-rigid registration step that requires manual landmark annotations.

Given the inherent difficulty involved in deriving trabecular bone anisotropy from clinical scans, and to circumvent the need for time-consuming registration procedures or manual landmark annotations, we proposed a supervised learning approach to predict trabecular bone anisotropy in the human proximal femur. Differently from previous approaches, we used a multi-output decision tree regressor that relies on a novel set of pose invariant feature descriptors. An implicit coordinate system of the proximal femur was constructed that enables computation of pose invariant features. Trabecular bone anisotropy was described as a tensor and its statistical relationship with the feature descriptors was learned from a database of aligned HRpQCT and clinical QCT pairs of images. We compared our approach to a registration based and PLS based approaches, and demonstrated on a set of leave-one-out experiments the ability of the approach to predict trabecular bone anisotropy from clinical QCT images.

2 Methods

Our aim is to establish a mapping from the pose invariant features $\boldsymbol{x} = (x_1, ...x_d) \in \mathbb{R}^d$ computed on clinical QCT to the corresponding tensor $\boldsymbol{y} \in \mathbb{R}^6$ computed on HRpQCT. Consequently the construction of the mapping is cast as a regression problem. Given a training set $\{\langle \boldsymbol{X_i}, \boldsymbol{Y_i} \rangle | i = 1, ..., N\}$ of N QCT and HRpQCT aligned pairs of images, we extract from each i_{th} image, $\boldsymbol{X_i} = (\boldsymbol{x}_1, ...\boldsymbol{x}_C) \in \mathbb{X}$ with an output response $\boldsymbol{Y_i} = (\boldsymbol{y}_1, ...\boldsymbol{y}_C) \in \mathbb{Y}$ over a grid of C nodes. We construct a function $\hat{\boldsymbol{y}} : \mathbb{X} \mapsto \mathbb{Y}$ from a space of images $\mathbb{X}$ to the space of responses $\mathbb{Y}$ that predicts the response for any new test image $\boldsymbol{X_{test}} \in \mathbb{X}$.

2.1 Feature Extraction

Implicit Coordinate System. For feature extraction, an implicit coordinate system of the proximal femur bone was constructed, and shown in Figure 1.

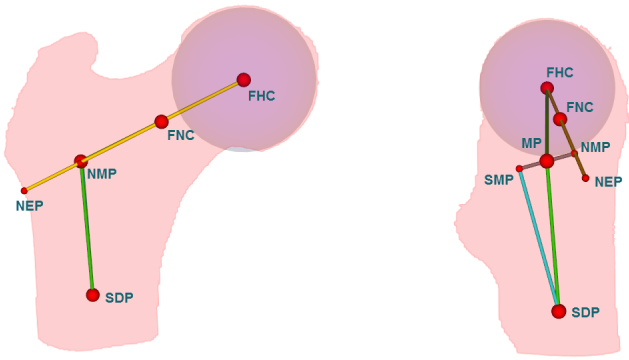

(a) Coronal view (b) Sagittal view

Fig. 1: Implicit coordinate system of the human proximal femur. It was used to extract a total of 10 morphometric pose invariant feature descriptors (see Table.1).

First, the center of the femoral head (FHC) was defined by a mass center of a spherical region with minimal cross-section area. The neck axis was constructed by following the procedure reported by Kang et al. [7, 8]. In short, the radius of the spherical region of the femoral head was enlarged by 25% and an initial neck center was defined. Using Powell's optimization, the center of the femoral neck (FNC) was computed and the neck axis was defined. The intersection point between the neck axis and the lateral surface of the proximal femur was defined as neck-axis-end-point (NEP). Then, the mass center of each slice distal to NEP was computed. The shaft axis was constructed by RANSAC fitting. The most distal point of the shaft axis was chosen as shaft-axis-distal-point (SDP). Since the neck and shaft axes does not intersect, a midpoint (MP) was defined as the shortest distance between the neck and shaft axes. By connecting SDP, MP and FHC, the implicit coordinate system was defined. The caput-collum-diaphyseal (CCD) angle was represented as $\angle(SDP)(MP)(FHC)$. All the images are re-positioned to the common coordinate system with origin at neck-midpoint (NMP), $+x$ axis as the neck axis and $+y$ axis towards the distal surface of the femur. From experiments, the procedure has shown to be robust, fast, and thus clinically applicable.

Input Features. A uniform sampling grid with isotropic grid spacing of $5.3mm$ [5] was defined over the QCT and HRpQCT images. At each node c_j of the grid $j = \{1, ...C\}$ lying inside the trabecular region, a volume of interest (VOI) was extracted on which feature descriptors and tensors (responses) were computed.

We propose to use two family of pose invariant features, morphometric- and texture-based. The morphometric features are computed with respect to the femoral implicit coordinate system [section 2.1]. We remark that in contrast to

Table 1: List of features computed at each grid node

Morphometric Features		**Texture Features**	
Scalar	**Angle**	**1st Order Statistics**	**GLCM**
Distance b/w FHC-FNC	CCD	Mean	Energy
Distance b/w FHC-MP		Std.Dev	Entropy
Distance b/w FNC-MP		Skewness	Correlation
Distance b/w FHC-c_j		Kurtosis	Inertia
Distance b/w FNC-c_j		Minimum	Cluster Shade
Distance b/w MP-c_j		Maximum	Cluster Prominance
Femoral Head Diameter			Inverse Difference Moment
Femoral Neck Min.Cross.Area			Haralick Correlation

previous approaches, this property results in a registration-free approach. The texture based features includes first order statistical features and GLCM [9, 10]. The list of features is presented in Table 1. The input feature set $\boldsymbol{x} = (x_1, ...x_d)$ includes all the morphometric features, mean and variance of all the texture features. For texture based features, a feature pooling was performed, followed by principal component analysis (PCA) to reduce dimensionality and redundancy of feature sets. This leads to a reduced feature space of $\mathbb{R}^{214}$ to $\mathbb{R}^{58}$.

Output Response. Tensors were computed on the corresponding VOI at each grid node c_j using the Mean Intercept Length technique (MIL) [11]. As tensors lie on a Riemannian manifold, we used the Log-Euclidean framework to perform Euclidean operations as follows [12]. The MIL tensor is a 3×3 positive semi-definite matrix $\boldsymbol{M}$ with associated eigenvectors $\boldsymbol{e_1}$, $\boldsymbol{e_2}$, $\boldsymbol{e_3}$ and eigenvalues λ_1,λ_2,λ_3. The matrix logarithm of $\boldsymbol{M}$ is calculated as

$$\boldsymbol{L} = \log(\boldsymbol{M}) = \sum_{k=1}^{3} \log(\lambda_k)(\boldsymbol{e_k} \otimes \boldsymbol{e_k}), \tag{1}$$

where $\otimes$ represents the dyadic product. The response variable is then defined as

$$\boldsymbol{y} = (L_{11}, L_{22}, L_{33}, \sqrt{2}L_{12}, \sqrt{2}L_{13}, \sqrt{2}L_{23}) \tag{2}$$

The tensor $\boldsymbol{M}$ can be obtained from the Log-Euclidean vector $\boldsymbol{y}$ by performing matrix exponential [12].

2.2 Multi-Output Regression Model

Decision forests are a group of learning methods widely used for classification and regression tasks in machine learning and computer vision. An extension of decision forest with extra trees algorithm has been proposed to handle multi-output image classification [13, 14]. We adopted this technique as a regression approach as it promotes preservation of tensor structure ($trace(\boldsymbol{M}) = 3$). During supervised learning, the algorithm randomly selects without replacement K

input variables $\{x_1, ...x_k\}$ from the training data $\boldsymbol{D} := \{\langle \boldsymbol{X_i}, \boldsymbol{Y_i} \rangle | i = 1, ..., N\}$. For each selected input variable, within the interval $[x_i^{min}, x_i^{max}]$ a cutpoint s_i was randomly defined and splitting $[x_i < s_i]$ was performed. Among the K candidate splits, the best split was chosen via optimizing the L2 mean square error [14]. This was a reasonable choice due to the Log-Euclidean transform being applied to the tensor.

3 Results and Discussion

3.1 Datasource

The study was performed on a database of QCT and HRpQCT images of human proximal femora. The training data comprises 30 femurs (15 males, 15 females with age 76±11 years, range 46-96) and were obtained from a previous study [15]. In summary, the clinical QCT images (Brillance64, Phillips, Germany, intensity: 100 mA, voltage: 120 kV, voxel size: 0.33 0.33 1.00 mm^3) and HRpQCT images (Xtreme CT, Scanco, Switzerland, intensity: 900 A, voltage: 60 kVp, voxel size: 0.082 0.082 0.082 mm^3). The clinical QCT images were resampled to have isotropic voxel spacing, and the cortical bone in the HRpQCT images was masked out according to the procedure reported in [16].

3.2 Evaluation Metric

For numerical evaluation of the proposed approach, a leave-one-out strategy was followed for the available 30 femurs. The MIL tensor $\boldsymbol{M}$ was measured from the HRpQCT images. The predicted tensor was represented as $\widehat{\boldsymbol{M}}$ with eigenvectors $\widehat{\boldsymbol{e_1}}$, $\widehat{\boldsymbol{e_2}}$, $\widehat{\boldsymbol{e_3}}$ and eigenvalues $\widehat{\lambda_1}$, $\widehat{\lambda_2}$, $\widehat{\lambda_3}$. We adopted the same evaluation metric described in [6]. The tensor norm error $TN_{error} = \|\boldsymbol{M} - \widehat{\boldsymbol{M}}\|/\|\boldsymbol{M}\|$, degree of anisotropy error $DA_{error} = |DA - \widehat{DA}|/DA$ and angular error of the principal tensor direction $PTD = \arccos(\boldsymbol{e_1}, \widehat{\boldsymbol{e_1}})$.

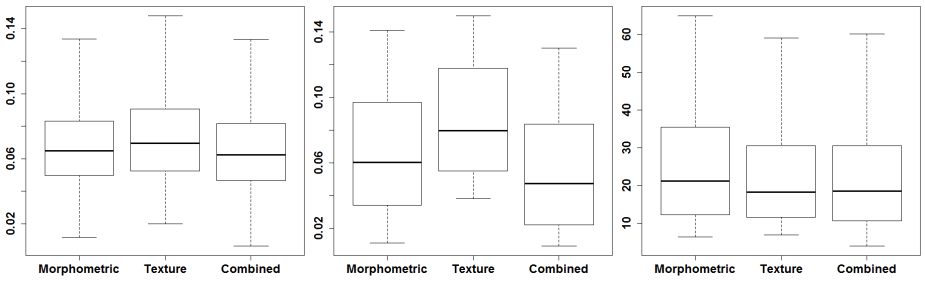

(a) TN Error (b) DA Error (c) PTD Error

Fig. 2: Prediction error of morphometric, texture and combined features for different evaluation metrics.

3.3 Experiment

Experiment 1: Feature Importance. On a first experiment, we evaluated the individual and combined predictive power of our feature descriptors. The number of trees used for the experiment was empirically found as 80. In comparison to the texture features, morphometric features offered a better tensor prediction and preservation of degree of anisotropy (Figure 2a, 2b). This supports the fact that trabecular bone anisotropy was related to the bone morphology. In contrast, texture features better predicted the principal tensor direction (Figure 2c). Trabecular bone anisotropy is characterized by specific orientations to support the stresses acting on the femur and they form an internal texture pattern. This motivated us to combine the features and perform the analysis. It resulted in a higher predictive power for the combined feature set (Figure 2).

Experiment 2: Comparative Study with Previous Approaches. On the second experiment, we compared the proposed approach to registration based- and PLS based approaches. For registration based, the image closest to the test image was taken and mapping was performed using rigid and non-rigid registration [17]. In the case of PLS based, the regression model was built using the proposed combined set of features. The number of trees used for the experiment was empirically found as 80. The prediction accuracy of our approach yielded comparable results to the registration based method and outperformed PLS based method (Figure 3a). In addition, a similar trend was observed for the degree of anisotropy (Figure 3b). Furthermore, our approach better predicted the principal tensor direction, which is of primary interest for finite element simulations (Figure 3c). The prediction accuracy in different regions of femur revealed that our approach offered a better prediction with lower tensor norm error (Figure 4). Further, it was able to track the main loading direction of the femur with higher accuracy.

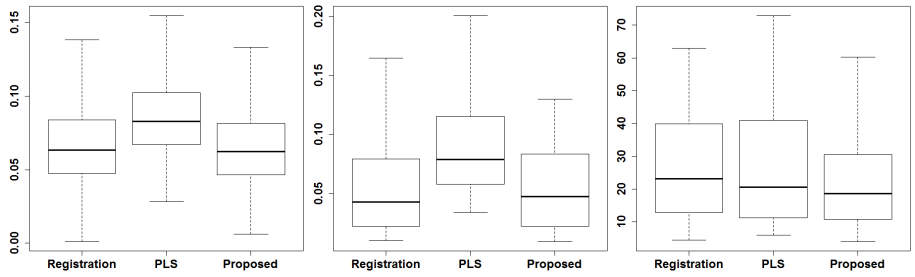

(a) TN Error (b) DA Error (c) PTD Error

Fig. 3: Prediction error of Registration-based, PLS-based and proposed approach for different evaluation metrics.

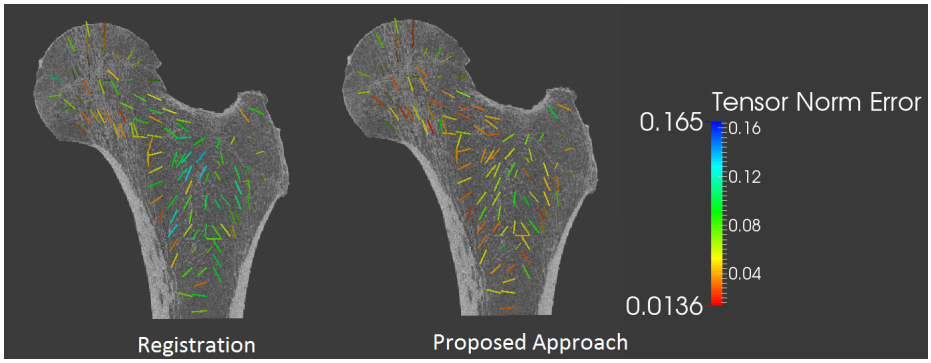

Fig. 4: Illustration of trabecular bone anisotropy prediction accuracy achieved on a test case. The lines indicate the principal orientation of the tensors computed on the HRpQCT image and displayed on an image slice. The colors correspond to the tensor norm error at each grid node. Left: tensor prediction accuracy by registration based approach, Right: tensor prediction accuracy by the proposed approach.

In comparison to the other approaches, the preference of the proposed approach can be explained by its ability of preserving tensor structure ($trace(\boldsymbol{M}) = 3$) and a prior knowledge of trabecular bone anisotropy over the entire population. This was supported by (Figure 4) that illustrates the possible problem of registration approach in handling highly homogenized bone areas.

4 Conclusion and Future Work

In finite element analysis, trabecular bone anisotropy contributes significantly to the assessment of the bone strength and improves diagnosis of musculoskeletal diseases [3, 4]. In comparison to previous approaches in predicting trabecular bone anisotropy, we propose a multi-output nonlinear supervised learning technique that uses pose invariant feature descriptors, which makes the approach registration-free. The nature of multi-output regression promotes preservation of tensor structure ($trace(\boldsymbol{M}) = 3$). According to our knowledge this is the first study predicting trabecular bone anisotropy from clinical QCT. The study also shows the potential of statistical approaches in predicting trabecular bone anisotropy. The approach can be extended to other anatomical sites where trabecular bone anisotropy plays an important role.

Future work includes a thorough comparison to other approaches on a larger dataset, incorporation of cortical information and evaluation through finite element analysis.

Acknowledgements. This work is supported by the Swiss National Science Foundation, Project number - 143769. The authors thank Dr. Ghislain Maquer for his comments on mechanical aspects and proof reading.

References

1. Kopperdahl, D.L., Aspelund, T., Hoffmann, P.F., Sigurdsson, S., Siggeirsdottir, K., Harris, T.B., Gudnason, V., Keaveny, T.M.: Assessment of incident spine and hip fractures in women and men using finite element analysis of CT scans. Journal of Bone and Mineral Research **29**(3) (2014)
2. Maquer, G., Musy, S.N., Wandel, J., Gross, T., Zysset, P.K.: Bone Volume Fraction and Fabric Anisotropy Are Better Determinants of Trabecular Bone Stiffness than Other Morphological Variables. Journal of Bone and Mineral Research (2014)
3. Enns-Bray, W.S., Owoc, J.S., Nishiyama, K.K., Boyd, S.K.: Mapping anisotropy of the proximal femur for enhanced image based finite element analysis. Journal of biomechanics **47**(13) (2014)
4. Hazrati Marangalou, J., Ito, K., Cataldi, M., Taddei, F., van Rietbergen, B.: A novel approach to estimate trabecular bone anisotropy using a database approach. Journal of biomechanics **46**(14) (2013)
5. Taghizadeh, E., Maquer, G., Reyes, M., Büchler, P.: Including the trabecular anisotropy from registered microCT data in homogenized FE model improves the bones mechanical predictions. In: CMBBE. (2014)
6. Lekadir, K., Hazrati-Marangalou, J., Hoogendoorn, C., Taylor, Z., van Rietbergen, B., Frangi, A.F.: Statistical estimation of femur micro-architecture using optimal shape and density predictors. Journal of biomechanics **48**(4) (2015)
7. Kang, Y., Engelke, K., Fuchs, C., Kalender, W.a.: An anatomic coordinate system of the femoral neck for highly reproducible BMD measurements using 3D QCT. Computerized medical imaging and graphics **29**(7) (2005)
8. Kang, Y., Engelke, K., Kalender, W.A.: A New Accurate and Precise 3-D Segmentation Method for Skeletal Structures in Volumetric CT Data. IEEE TMI **22**(5) (2003)
9. Haralick, R.M., Shanmugam, K.: Textural Features for Image Classification. IEEE TSMC-3 **6** (1973)
10. Ortiz, A., Palacio, A.A., Górriz, J.M., Ramírez, J., Salas-González, D.: Segmentation of brain MRI using SOM-FCM-based method and 3D statistical descriptors. Computational and mathematical methods in medicine (2013)
11. Harrigan, T., Mann, R.: Characterization of microstructural anisotropy in orthotropic materials using a second rank tensor. Journal of Materials Science **19**(3) (1984)
12. Pennec, X., Fillard, P., Ayache, N.: A Riemannian Framework for Tensor Computing. International Journal of Computer Vision **66**(1) (2006)
13. Dumont, M., Marée, R.: Fast multi-class image annotation with random windows and multiple output randomized trees. Proc. of VISAPP **2** (2009)
14. Marée, R., Wehenkel, L., Geurts, P.: Extremely randomized trees and random subwindows for image classification, annotation, and retrieval. Decision Forests for Computer Vision and Medical Image Analysis (2013)
15. Dall'Ara, E., Luisier, B., Schmidt, R., Kainberger, F., Zysset, P., Pahr, D.: A nonlinear QCT-based finite element model validation study for the human femur tested in two configurations in vitro. Bone **52**(1) (2013)
16. Pahr, D.H., Zysset, P.K.: From high-resolution CT data to finite element models: development of an integrated modular framework. CMBBE Journal **12**(1) (2009)
17. Klein, S., Staring, M., Murphy, K., Viergever, M.A., Pluim, J.P.W.: elastix: A toolbox for intensity-based medical image registration. IEEE Trans. Med. Imaging **29**(1) (2010)